Materials Advances

ROYAL SOCIETY OF CHEMISTRY

PAPER

View Article Online
View Journal | View Issue

Cite this: *Mater. Adv.*, 2025, 6, 6022

A 3-in-1 multifunctional porous organic polyimide: detection, capture and controlled release of antibacterial drugs†

Rasha Diab,[ab] Fatima Mahroos,[b] Sreeshna Ravindran,[b] Oussama M. El-Kadri*[abc] and Mohammad H. Al-Sayah *[abcd]

Two imide-linked porous organic polymers (POPs), PI-POP and NI-POP, were synthesized and evaluated as multifunctional materials for chemical sensing, adsorption, and temperature-responsive release applications. Characterization revealed hierarchical porosity, with surface areas of 723 m^2 g^{-1} for PI-POP and 385 m^2 g^{-1} for NI-POP. Their π-rich frameworks enabled strong fluorescence-based detection of tetracycline (TC) as a probe molecule. PI-POP showed stronger quenching behavior, aligning with the Lehrer model, while NI-POP followed Stern–Volmer dynamics. Beyond sensing, the adsorption behavior of tetracycline was systematically investigated under various conditions, including pH, initial drug concentration, adsorbent dose, and contact time. Optimal removal was observed under neutral pH, with PI-POP achieving ~90% TC removal at a solid–liquid ratio of 1.5. The higher surface area and pore volume of PI-POP explain its superior uptake capacity and promote it as a more effective adsorbent. Both polymers followed the Elovich model in kinetic studies and aligned with Freundlich (PI-POP) and Temkin (NI-POP) models in isothermal analysis. Comparable removal efficiencies in tap water and buffered systems confirmed their robustness and practical applicability. Furthermore, controlled release tests at physiological temperature showed faster TC release from NI-POP, likely due to weaker host–guest interactions, making it suitable for short-term delivery applications. The released TC exhibited a clear inhibition zone against both *E. coli* and *S. epidermidis*. This confirms the retained antibacterial activity and structural integrity of TC post-release. This work highlights the potential of tailored POPs for integrated environmental and biomedical applications.

Received 8th June 2025,
Accepted 14th July 2025

DOI: 10.1039/d5ma00611b

rsc.li/materials-advances

1. Introduction

Antibiotic-contaminated wastewater poses a significant environmental concern, particularly due to the persistence of these compounds and their role in fostering antibiotic-resistant and multi-drug-resistant bacteria.[1] Despite their effectiveness in the treatment and prevention of diseases caused by bacterial infections, the extensive usage of antibiotics in agriculture leads to inevitable introduction into wastewater systems.[2,3] Key sources of antibiotic contamination include agriculture runoff, hospital waste and pharmaceutical industry effluents.[2,4] The persistence of antibiotics in aquatic environments disrupts microbial ecosystems by exerting selective pressure on susceptible bacteria.[5] This gives rise to antibiotic-resistant strains, rendering current treatments less effective.[6,7] Moreover, these contaminants can infiltrate human and animal microbial ecosystems through consumption *via* the food chain and drinking water.[8]

To effectively address this escalating issue, it is essential to develop integrated approaches that go beyond the detection and removal of antibiotics from water systems, encompassing their sustainable reuse. Advances in sensing technologies have introduced several detection methods including microbiological assays, liquid chromatography-mass spectrometry, electrochemical sensors, and fluorescence-based systems.[9] While microbiological assays are time-consuming and lack sensitivity,[10] spectroscopic methods are often costly and complex; and electrochemical sensors often fall short in stability and accuracy.[9] Recently, luminescent sensor-based analysis has gained

[a] *Materials Science and Engineering Program, College of Arts and Sciences, American University of Sharjah, POB 26666, Sharjah, United Arab Emirates. E-mail: oelkadri@aus.edu, malsayah@aus.edu*
[b] *Department of Biology, Chemistry, and Environmental Sciences, American University of Sharjah, POB 26666, Sharjah, United Arab Emirates*
[c] *Materials Research Center, American University of Sharjah, POB 26666, Sharjah, United Arab Emirates*
[d] *Advanced Biosciences and Bioengineering Research Center, American University of Sharjah, P.O. Box 26666, Sharjah, United Arab Emirates*

† Electronic supplementary information (ESI) available. See DOI: https://doi.org/10.1039/d5ma00611b

attention due to its key advantages such as high sensitivity, real-time response, simplified procedures, and cost efficiency.[11]

Following detection, efficient removal strategies are crucial to mitigate the negative impact of persistent antibiotics. Techniques such as photocatalytic degradation,[12] microbial degradation,[13] and adsorption[14] have been developed. Among these, adsorption stands out due to its simplicity, high efficiency, and resource availability.[15] Furthermore, moving beyond conventional remediation, enabling the controlled release of captured antibiotics offers the potential for their reuse as therapeutic agents. Recent advances in stimuli-responsive multifunctional nano-biomaterials, such as biopolymer-based composites, metal nanoparticles and mesoporous carbon nanospheres,[16] have demonstrated promising potential for integrated removal and delivery systems.[17] However, their practical use is hindered by weak mechanical properties, poor aqueous stability, and challenges in scalability and toxicity concerns.[16,18] These limitations have accelerated the search for more chemically and structurally robust systems.

In this context, porous organic polymers (POPs), which are amorphous three-dimensional network materials constructed from diverse covalently bonded organic building blocks and characterized by well-defined porosity, have emerged as promising candidates to serve a multifunctional role.[19,20] Their intrinsic features—including structural diversity, high chemical and thermal stability, substantial porosity and surface areas, tunable structures, metal-free nature, and ease of functionalization[21]—allow the integration of multiple functionalities into a single platform.

The incorporation of chromophoric entities within their structures renders POPs highly effective as fluorescent sensors[22] capable of detecting antibiotic residues, while their porous and chemically versatile frameworks support efficient adsorption capabilities.[23] Notably, with appropriate molecular design, POPs can also be engineered to allow stimuli-responsive drug release under physiological conditions.[24] In this context, tetracycline (TC), a widely used broad-spectrum antibiotic,[25] was selected as a representative probe molecule due to its environmental relevance and persistence in aquatic systems. Consequently, TC serves as a suitable model for investigating the multifunctional performance of POPs in antibiotic detection, capture and release.

In this study, we report the synthesis of two imide-linked porous organic polymers, PI-POP and NI-POP, designed for multipurpose applications. These polymers possess π-rich networks comprising triazine rings, imide functionalities, and phenyl groups, which impart fluorescence sensitivity and promote strong host–guest interactions. Their potential, as chemical sensors, was demonstrated through fluorescence titration with TC, where both polymers exhibited notable quenching responses. PI-POP, in particular, showed stronger fluorescence turn-off. Following detection, the adsorption capabilities of the polymers were systematically evaluated in buffer solutions. Both materials feature hierarchical micro-mesoporosity—facilitating efficient TC uptake. PI-POP achieved a higher adsorption capacity, likely due to stronger binding interactions with TC. The removal efficiency increased with higher adsorbent doses, with PI-POP achieving ~90% TC removal. Comparable results in tap water validated their applicability under realistic environmental conditions.

Importantly, the study also explored the sustainable reuse of the captured TC through controlled release experiments conducted at physiological temperature (37 °C), showing that TC retained its antibacterial activity upon release, effectively inhibiting *Staphylococcus epidermidis* (SE) and *Escherichia coli* (EC), with NI-POP exhibiting a more pronounced drug release. These findings underscore the multifunctional potential of PI-POP and NI-POP, presenting a holistic solution encompassing detection, removal, and sustainable reuse of antibiotics.

2. Materials and methods

2.1. Materials

All solvents, starting materials, and reagents were purchased from Sigma-Aldrich (Germany) and used as received unless otherwise specified. Tetracycline hydrochloride (TC) was used in this study. 1,4-Bis-(2,4-diamino-1,3,5-triazine)-benzene (BATB) was synthesized following a previously reported procedure.[26] Our group has recently reported the synthesis of the naphthalene-based polyimide NI-POP.[27] Building on the same protocol, we now report the synthesis of a novel polyimide derived from the same amine precursor (BATB) with pyromellitic dianhydride (PMDA) *via* an imidization reaction.

2.2. Instrumentation

Fourier transform infrared (FT-IR) spectroscopy was performed using a Shimadzu IRTracer-100 spectrometer equipped with a single reflection attenuated total reflectance (ATR) accessory. The thermal stability of the synthesized polymers was assessed with a Perkin thermogravimetric analyzer (TGA) at a heating rate of 5 °C min^{-1} under nitrogen flow. Scanning electron microscopy (SEM) images were captured using a TESCAN-LMU field emission scanning electron microscope in ultra-high mode to investigate the morphology of polymers. Powder X-ray diffraction (PXRD) patterns were obtained with a Panalytical X'pert3 Pro multipurpose diffractometer using Cu Kα radiation over a 2θ range of 5–50°. Nitrogen adsorption–desorption measurements at 77 K were performed using a Quantachrome analyzer to evaluate the surface area and pore width and volume. The surface area was calculated using the Brunauer–Emmett–Teller (BET) method, while the pore size distribution (PSD) was analyzed using the density functional theory (DFT) method, and the pore volume was obtained by the single point pore volume method at a relative pressure P/P_0 of 0.95. The concentration of tetracycline solutions was determined using a UV-Vis spectrometer (Shimadzu UV-1800) with a quartz cuvette and calculated according to calibration curves. Photoluminescence measurements were performed using an Edinburgh Instruments FLS-900 scanning spectrofluorometer. Zeta potential measurements were conducted using a Litesizer 500 particle analyzer (Anton Paar).

2.3. Methods

2.3.1. Synthesis of PI-POP. PI-POP was synthesized similarly to NI-POP. BATB (3.0 mmol, 0.89 g) and PMDA (6.0 mmol,

1.3 g) were added to a flask containing 15 mL of freshly distilled dimethyl sulfoxide (DMSO). The solution was stirred at room temperature under argon for 30 min, then 0.7 mL of toluene was added to the mixture. The imidization reaction was conducted at 180 °C for 72 hours. The precipitate was filtered and washed thoroughly with tetrahydrofuran (THF), dichloromethane (CH_2Cl_2) and acetone. The residue was soaked in chloroform for 24 h, filtered, washed with CH_2Cl_2, and dried in an oven overnight at 80 °C, yielding PI-POP in the form of a white colored powder (1.72 mg, yield: 87%).

2.3.2. Luminescence sensing. Fluorescence titration experiments were conducted to assess the potential of PI-POP and NI-POP as chemical sensors for detecting TC. Each polymer (1 mg) was suspended in 10 mL of PBS and sonicated for 40 min. Their fluorescence emission was recorded at $\lambda_{excitation}$ = 310 nm. Subsequently, incremental additions (5 μL to 1000 μL) of TC solution were introduced into the polymer suspensions, ensuring that the polymer concentration remained constant throughout the titration process. Fluorescence emission intensities were measured before (I_0) and after (I) each TC addition. The quenching behavior was analyzed using the Stern–Volmer (SV) model, plotting I_0/I *versus* TC concentration to elucidate the interaction mechanisms between the polymers and TC.

2.3.3. Adsorption studies. A tetracycline (TC) solution with a concentration of 50 mg L^{-1} was prepared by dissolving 2.5 mg of tetracycline hydrochloride in 50 mL of a buffer solution. Separate solutions were prepared using different buffers to achieve the desired pH levels: acetate buffer (pH 4), phosphate-buffered saline (PBS; pH 7.5), and bicarbonate buffer (pH 8.5). To study the effect of pH, 5 mL of each prepared TC solution was taken, and then 5 mg of either PI-POP or NI-POP was added to the 5 mL aliquot. The mixtures were shaken in a ThermoShaker at 25 °C for 4 h. The initial and final concentrations of TC were determined using a dual-beam UV-Vis spectrophotometer, measuring absorbance at wavelengths corresponding to each buffer medium: 358 nm for acetate, 363 nm for PBS, and 373 nm for bicarbonate. Calibration curves were used to quantify TC concentrations. Adsorption capacities (q_e, mg g^{-1}) and percentage removal efficiencies (E%) were calculated using eqn (S1) and (S2), respectively (Table S1, ESI†).

To evaluate the effect of adsorbent dosage, varying amounts of the adsorbent (0.5 to 15 mg) were added to 10 mL of TC solution in PBS (50 mg L^{-1}). The mixtures were shaken at 25 °C until equilibrium was reached. Initial and equilibrium TC concentrations were measured, and q_e and E% were calculated as described above.

For the effect of contact time, 10 mg of each POP was added to 20 mL of TC solution in PBS (50 mg L^{-1}). The mixtures were shaken at 25 °C. Aliquots were taken at predetermined intervals over 28 hours. The residual TC concentrations were measured, and q_e and E% were calculated.

Adsorption isotherms were studied by adding 10 mg of each POP to 20 mL of TC solution in PBS with varying initial concentrations. The mixtures were shaken at 25 °C for 48 hours. Initial and equilibrium TC concentrations were determined, and similarly, q_e and E% were calculated.

2.3.4. Adsorption kinetics and isotherm modelling. Several models are employed in adsorption kinetics to describe the rate at which adsorbates adhere to surfaces. In this study, three widely used models—the pseudo-first-order, pseudo-second-order, and Elovich models—were applied in both linear and nonlinear forms.

Similarly, adsorption isotherms describe the relationship between the amount of adsorbate retained on the adsorbent surface (q_e) and its concentration (C_e) at equilibrium under constant temperature. The experimental data were fitted using three established isothermal models—the Langmuir, Freundlich, and Temkin models—also in both linear and nonlinear forms.

Detailed explanations of each model and the corresponding equations are provided in the ESI.†

2.3.5. Adsorption in tap water. To evaluate the performance of the adsorbents in complex media, adsorption experiments were conducted in tap water using a TC solution with an initial concentration of 50 mg L^{-1}. The removal efficiency in tap water was compared with that in PBS to assess the impact of complex media on the adsorption behavior. The tap water used was sourced from the laboratory sink.

2.3.6. Controlled release and antibacterial activity of the TC-loaded POPs. To evaluate the release behavior of tetracycline from the synthesized POPs under different thermal conditions, 1.5 mg of the loaded polymer was dispersed in 3 mL of PBS (pH 7.4) and incubated at either room temperature (RT) or physiological temperature (37 °C). UV-vis absorbance measurements were conducted at predefined intervals over a 10-hour period to monitor the cumulative release of TC. 1 mL of the solution was withdrawn and replaced with an equal volume of fresh PBS at 1-hour intervals to maintain a consistent volume and concentration gradient.

The antibacterial activity of the TC-loaded POPs was determined against SE and EC bacteria, respectively, using the agar diffusion test. A sample (1 mg) of each TC-loaded polymer was placed in a Petri dish seeded with the bacterial strain, covered with a wet paper disc, and incubated for 24 h. The diameter of growth inhibition of the bacteria was then measured and compared to a positive control (TC disc; 30 μg TC) and a negative control (unloaded polymer; 1 mg). Studies were conducted in triplicate.

3. Results and discussion

3.1. Synthesis and characterization of POPs

We have recently reported[27] the synthesis of an imide-linked porous polymer, NI-POP, using an imidization reaction between BATB and the naphthalene-1,4,5,8-tetracarboxylic dianhydride (NTDA) precursor, as depicted in Scheme 1. In this study, a second polymer, PI-POP, was synthesized using a similar approach but employing a different anhydride precursor (PMDA). The use of this smaller, more compact aromatic building block was intended to enhance the surface area.[28] As reported in previous studies,[29,30] shorter linkers reduce conformational flexibility and interpenetration between polymer

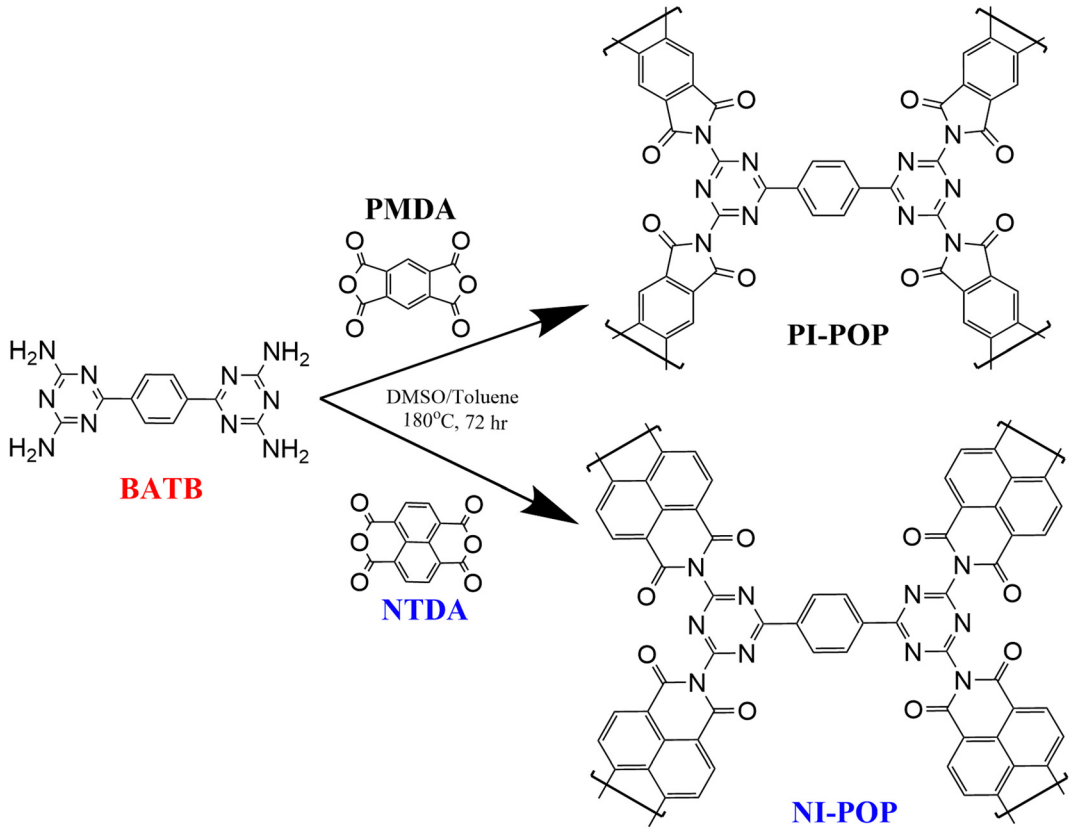

Scheme 1 Synthetic route for PI-POP and NI-POP.[27]

chains, thereby minimizing space filling and preserving microporosity, leading to an increase in surface area.

Both polymers were strategically designed to incorporate chromophoric building blocks, enabling their use in fluorescence-based sensing. The afforded polymers are insoluble in common organic solvents, which facilitates their purification and highlights their robust interconnected network. Various spectroscopic and analytical techniques were used to characterize the polymers. FTIR spectroscopy confirmed the successful synthesis of PI-POP, with spectra from two independently prepared batches (Fig. S1, ESI†) showing excellent consistency and demonstrating the reliability of the synthetic protocol.

Fig. 1A and Fig. S1A (ESI†) show that the bands corresponding to the stretching of the –NH of the primary amine, falling in the range of 3140–3420 cm^{-1}, as well as the band at 1629 cm^{-1} referring to the in-plane bending of –NH, disappeared. The triazine's quadrant band and semi-circle stretching bands are observed at 1527 and 1469 cm^{-1}, respectively, confirming the conversion of the amine functionalities and the successful incorporation of the triazine moieties of BATB in the structure.[31] Moreover, the carbonyl symmetrical stretching band shifted to 1716 cm^{-1} in comparison to the corresponding anhydride.[32] This is attributed to the conversion of the anhydride (–CO–O–CO–) to imide (–CO–N–CO–). The disappearance of the multiple bands (from 1100 to 1300 cm^{-1}) corresponding to the C–O stretching of the anhydride[33] and the emergence of the imide ring stretching bands at 1226 and 1369 cm^{-1},[34] along with its deformation band at 731 cm^{-1}, further endorse the conversion of the anhydride ring to the imide ring.[32,35]

In terms of thermal stability, the TGA curve of PI-POP (Fig. 1B) showed a 13% weight loss up to 80 °C, which is attributed to the evaporation of trapped solvent molecules. The polymeric network remained stable up to approximately 275 °C, with an additional 11% weight loss observed. Beyond this point, continuous degradation of the network was noted. It is worth noting that NI-POP demonstrated higher thermal stability, remaining stable up to 375 °C. This enhanced thermal stability is likely due to the presence of an additional phenyl unit in its structure, which promotes stronger π–π stacking between the polymeric chains.

PI-POP and NI-POP exhibit an amorphous nature, as shown by XRD data (Fig. S1B, ESI†). The absence of sharp peaks and the presence of only a broad peak centered around 21°–22° are characteristic of many amorphous POPs.[36] SEM images of PI-POP revealed a morphology comparable to that of NI-POP, given their similar chemical structures. PI-POP exhibited a coarse surface and porous texture on the microscale (Fig. 1C). At higher magnification (Fig. 1D), nearly spherical particles with an average diameter of 35 nm were observed, similar to those found in NI-POP.

Porosity studies were conducted to analyze their textural features, revealing that both polymers exhibited similar isotherm behavior despite differences in BET surface area, with PI-POP and NI-POP displaying hybrid isotherm types. N_2 adsorption–desorption isotherms of PI-POP (Fig. 2A) demonstrated an

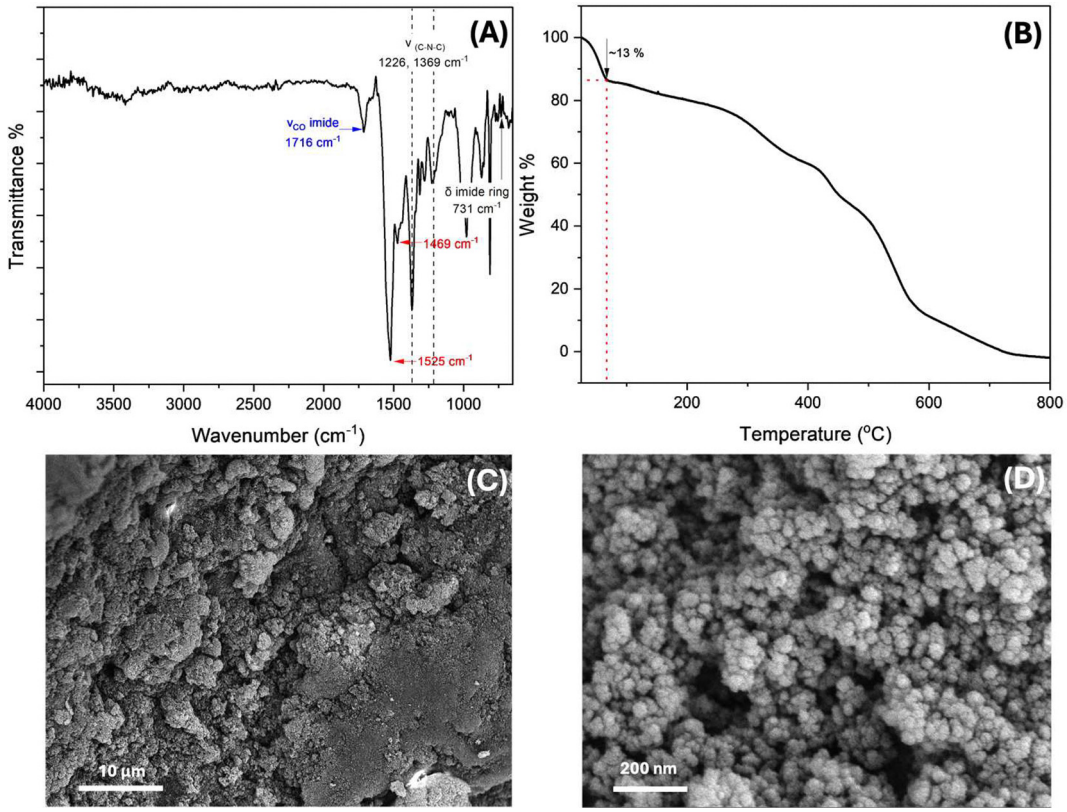

Fig. 1 Characterization of PI-POP using various techniques: FT-IR spectrum for chemical structure identification (A), TGA curve for thermal stability (B), and SEM images (C) and (D) at different scales showing morphological features.

increase in the nitrogen gas uptake at low relative pressure, indicative of micropore filling (type I isotherm), followed by a gradual uptake at higher relative pressure,[37] specifically the steep increase at $P/P_0 > 0.9$, suggesting the presence of mesopores (type II isotherm)[38] with the presence of a hysteresis loop.

Table 1 summarizes the textural characteristics of both polymers. The BET surface areas of PI-POP and NI-POP were 723 $m^2\ g^{-1}$ and 385 $m^2\ g^{-1}$, respectively. The hybrid porosity was further supported by the pore size distribution calculated using the DFT method, which showed a dominant pore size centered at 1.23 nm for both polymers, along with a relatively small mesopore (>2 nm) volume, highlighting the mixed pore structure (Fig. 2B). The single-point pore volume method calculated at P/P_0 = 0.95 showed a total pore volume of 1.201 $cm^3\ g^{-1}$ for PI-POP, approximately twice that of NI-POP. The discrepancy observed in surface area and pore volume further supports the design strategy of incorporating a smaller dianhydride monomer in PI-POP. This pre-design approach

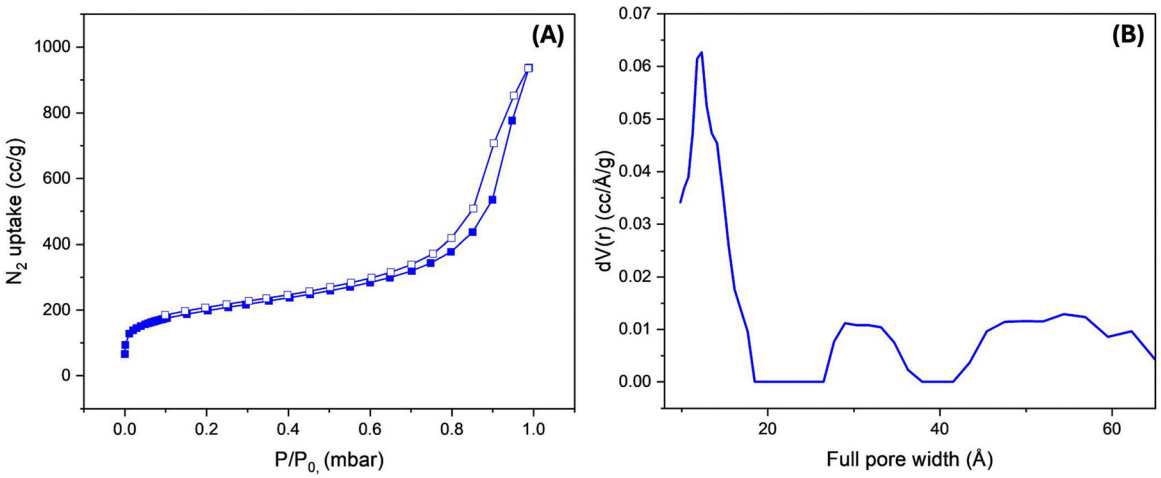

Fig. 2 Nitrogen adsorption–desorption isotherms (A) and PSD curve (B) of PI-POP.

Table 1 Porosity features of both polymers

Polymer	S_{BET}[a] ($m^2\ g^{-1}$)	Pore volume[b] ($cm^3\ g^{-1}$)	Dominant pore[c] size (nm)	Range of mesopore size (nm)
PI-POP	723	1.201	1.23	2–6
NI-POP	385	0.6042	1.23	2–6

[a] BET surface area. [b] Pore volume calculated at $P_0/P = 0.95$. [c] Dominant pore size obtained by DFT calculations.

indeed resulted in a more porous framework, demonstrating enhanced overall porosity.

Owing to their hierarchical porosity, structural stability, diverse chemical functionalities, and richness in conjugated frameworks encompassing light-responsive units, both POPs were first evaluated for their potential as efficient chemical sensors for tetracycline.

3.2. Luminescence sensing of TC

Early detection of TC at low concentrations is essential for environmental monitoring. In this context, both POPs were investigated for their potential as efficient fluorescence-based chemical sensors. Each polymer was suspended in PBS and exhibited significant fluorescence emission: PI-POP displayed an emission peak centered at ~510 nm, while NI-POP had a peak around 345 nm, both with an excitation wavelength of 310 nm (Fig. 3). The photoluminescence of these polymers originates from their π-conjugated skeletons composed of rigid aromatic rings.[39]

Prior to titration with TC, the emission spectrum of each polymer was monitored over time to confirm the stability of their intrinsic fluorescence. This ensured that any subsequent changes in emission intensity could be attributed solely to interactions with TC during titration. Emission intensities were recorded before (I_0) and after (I) incremental additions of TC solution, while maintaining a constant polymer suspension concentration throughout the titration process.

In Fig. 4A and B, both polymers exhibit a decrease in emission intensity as the concentration of TC increases from 0 to 10 mg L^{-1} (equivalent to 0–22.5 μM). To analyze this luminescence quenching, a Stern–Volmer (SV) plot of I_0/I *versus* [TC] was employed. The two porous polymers display distinct behaviors. The SV plot for NI-POP shows a perfect linear increase, indicating a consistent quenching effect proportional to the TC concentration. This linearity is confirmed by a high correlation coefficient ($R^2 >$ 0.99), suggesting mainly a dynamic (collisional) quenching between NI-POP and TC molecules[40] (Fig. 4F). Collisional quenching refers to the interaction between an excited-state fluorophore and a ground-state quencher during the fluorophore's excitation lifetime. This interaction leads to the formation of a transient complex, which subsequently dissociates through a non-radiative relaxation process.[41] As a result, the number of emitted fluorescence photons decreases, reducing the overall fluorescence intensity. In contrast, the SV plot of PI-POP deviates from linearity, exhibiting a downward curvature (Fig. 4C). A linear fit of the SV model yields an R^2 of 0.90 (Fig. 4D), indicating a less consistent

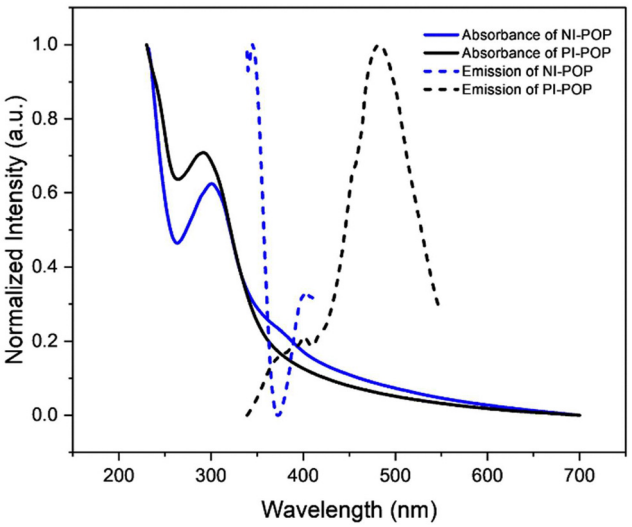

Fig. 3 UV-Vis absorbance and emission (at $\lambda_{excitation}$ = 310 nm) spectra of both POPs.

quenching response. This deviation suggests a more complex interaction mechanism between PI-POP and TC.

To better understand the sensing behavior of PI-POP, the Lehrer equation—a modification of the standard SV equation—was applied (eqn (S10), Table S1, ESI†). This model accounts for complex porous systems with two distinct populations of fluorophores: one accessible to analytes and the other inaccessible.[40] The application of the Lehrer equation provided a linear fit that closely aligned with the experimental data for PI-POP ($R^2 > 0.99$; Fig. 4E), explaining the observed saturation effect at higher TC concentrations due to accessible-site saturation.

To understand the actual quenching mechanism of PI-POP, further investigations were conducted. As shown in Fig. S2A (ESI†), the absorbance spectrum of TC and the emission spectrum of PI-POP exhibited no significant overlap, ruling out the internal filtration effect (IFE) mechanism.[42] To probe molecular interactions, UV-Vis absorbance spectra of pure components were compared with that of the mixture. After subtracting the absorbance of PI-POP, a redshift in the TC absorption peak from 275 nm to ~286 nm was observed in the mixture (Fig. S2B, ESI†). This shift, indicating an alteration in the electronic structure, is most likely due to hydrogen bonding interactions leading to formation of a complex[43,44] between ground-state PI-POP and TC molecules at high concentrations, likely causing static quenching. In addition to strong π–π interactions,[45] the formation of PI-POP complexes with TC *via* hydrogen bonding[46] was verified by FTIR spectroscopy through comparison of the spectra of pristine polymers with those of TC-loaded samples. As illustrated in Fig. S3 (ESI†), the TC-loaded PI-POP retains the key structural bands of the pristine polymer but with notable shifts and additional features. Specifically, a reduced intensity and a slight shift of the carbonyl peak around 1714 cm^{-1} were observed, along with a redshift of the triazine bands (at ~1527 and 1465 cm^{-1}) and the imide group (~1369 cm^{-1}). As proved by IR, the triazine rings, rich in nitrogen sites,[39] significantly facilitated the adsorption. An

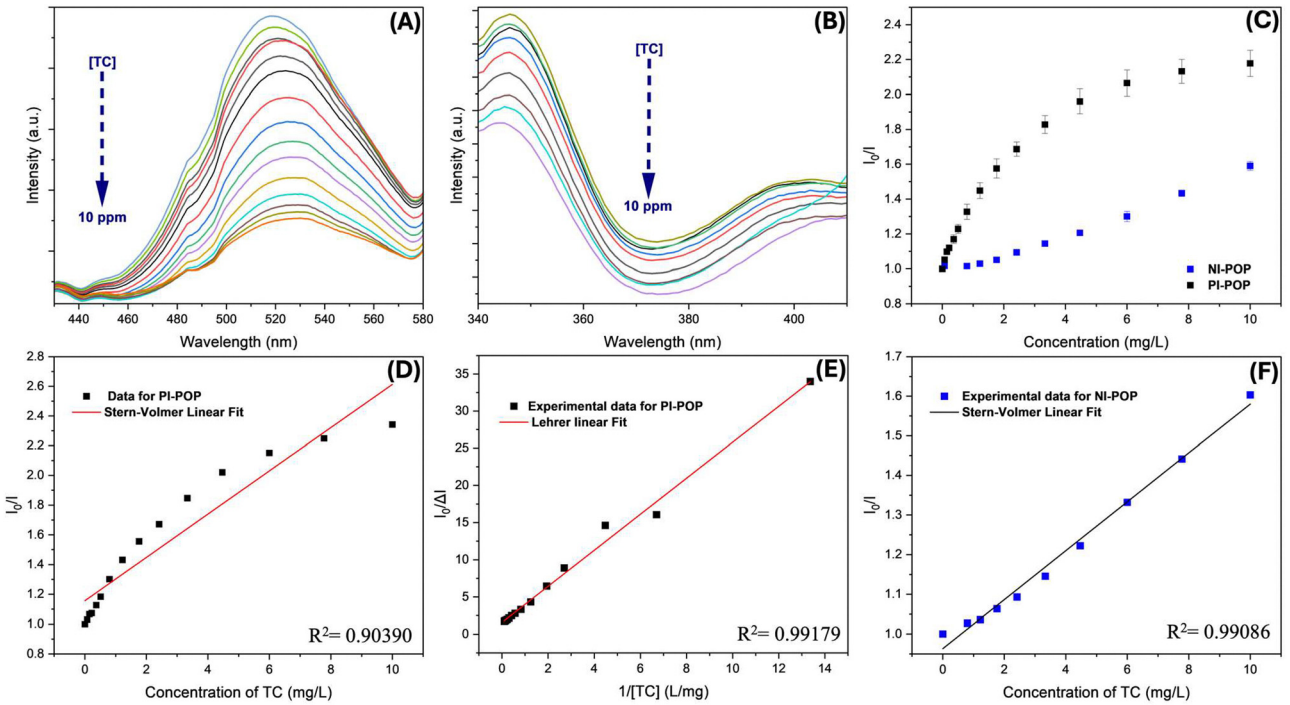

Fig. 4 Changes in the fluorescence intensity ($\lambda_{excitation}$ = 310 nm) of PI-POP (A) and NI-POP (B) upon titration with tetracycline; correlation between I_0/I and TC concentration in suspensions of polymers (C); the Stern–Volmer linear fit for PI-POP (D) and NI-POP (F); the Lehrer linear fit for PI-POP (E).

additional broad band in the 3200–3600 cm^{-1} region, corresponding to O–H/N–H stretching vibrations, was also observed.[47,48] This band, not existing in the spectrum of pure PI-POP, signifies the presence of hydrogen bonding, which altered the local chemical environment of the polymer.

As a result, the formation of an increasing number of these non-fluorescent complexes may not only cause static quenching but also sterically hinder additional analyte molecules from accessing inner pores, further resulting in quenching saturation. This supports the observed deviation from linearity in the Stern–Volmer plot.

Compared to NI-POP, PI-POP demonstrated a greater change in fluorescence emission at the same TC concentration. At 10 ppm TC, the I_0/I ratio for PI-POP is 2.3, whereas for NI-POP it is 1.6 (Fig. 4C). To quantify the quenching effect, K_{sv} was calculated. For NI-POP, K_{sv} (slope in SV eqn (S9), Table S1, ESI†) was equal to $(2.96 \pm 0.10) \times 10^4$ L mol^{-1}, suggesting a high quenching effect.[49] On the other hand, K_{sv} for PI-POP, calculated from the Lehrer equation (K_{sv} = intercept/slope; eqn (S10), Table S1, ESI†), was $(3.15 \pm 0.55) \times 10^5$ L mol^{-1}, one order of magnitude higher than that of NI-POP. These findings emphasize enhanced binding interactions between PI-POP and TC molecules, likely due to a larger number of interactive sites within the structure of PI-POP. Moreover, the fraction of accessible fluorophores (f, as defined in eqn (S10), ESI†) was determined to be 0.63. This analysis confirms that, despite the higher surface area and pore volume of PI-POP, not all fluorophore sites are accessible to TC molecules.

In summary, the response of PI-POP appears more complex due to the heterogeneous accessibility of pore/sites and its higher density of interactive centers available for TC binding.

3.3. Adsorption of TC

Beyond the detection of antibiotic contaminants, it must be followed by effective strategies to eliminate them from the environment. Therefore, in the second part of this study, the adsorption performance of the synthesized POPs was systematically evaluated to assess their ability to capture and retain tetracycline from buffer and complex media. Key parameters affecting adsorption efficiency—including solution pH, adsorbent dosage, contact time and initial TC concentration—were thoroughly investigated to optimize the removal process.

3.3.1. Impact of pH. The solution pH plays a critical role in the adsorption process, as it can influence both the surface charge of the adsorbent and its ionization behavior.[50] Tetracycline is an amphoteric chemical due to the presence of a dimethylammonium group (C4), a phenolic diketone moiety (C10–C12), and a tricarbonyl system (C1–C3).[51] Accordingly, TC exists in distinct forms depending on the pH: as a cation at pH levels below 3.3, a zwitterion between pH 3.3 and 7.7, and an anion at pH levels above 7.7.[52] Each polymer (5 mg) was added to a TC solution (50 mg L^{-1}) prepared in acetate (pH = 4), PBS (pH = 7.5), and bicarbonate (pH = 8.5) buffers. Under identical experimental conditions (shaking, time of contact, and temperature), aliquots of each solution were taken after 4 hours of shaking, and the residual TC concentration was determined *via* UV-Vis spectrophotometry.

As shown in Fig. 5A, the highest adsorption capacity was observed in PBS, followed by acetate, and the lowest capacity was recorded in bicarbonate. This trend aligns with the expected behavior, as under acidic conditions competition between protons and the TC^+ species limits site occupancy on the adsorbent surface.[23] NI-POP demonstrated higher efficiency

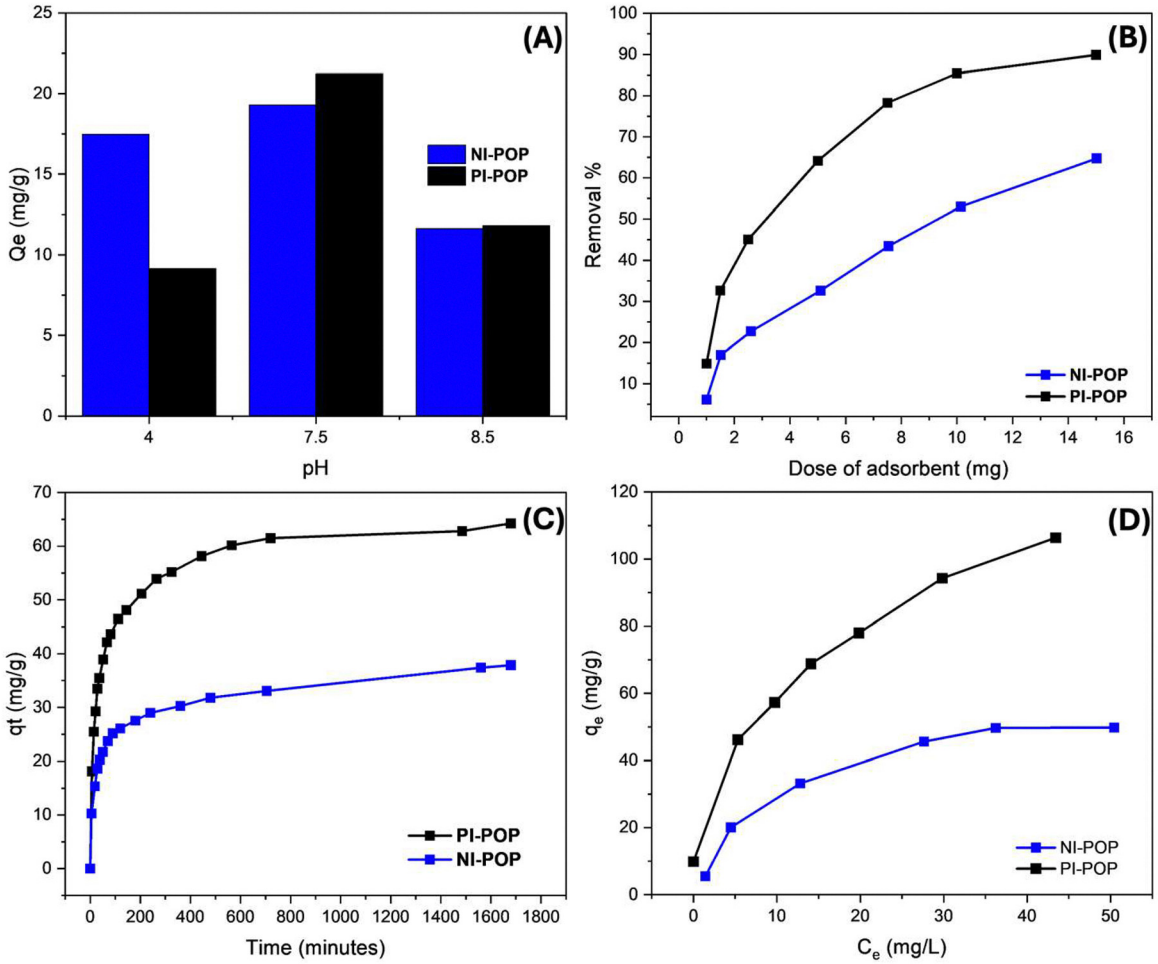

Fig. 5 Loading capacity of TC solution by PI-POP and NI-POP at different pH values (A), different dosages of the polymer (B), the kinetic study (C), and isotherms recorded over a range of TC concentrations (D) in PBS.

than PI-POP only in acetate, despite its lower surface area. To understand this behavior, zeta potential measurements (Table S2, ESI†) were conducted for both polymers. As NI-POP showed a pH-dependent surface charge, its enhanced adsorption of TC in acetate was attributed to its overall negative surface charge, favoring electrostatic attraction with TC^{+}, while PI-POP carried a positive charge, leading to repulsion. Under neutral conditions, the ionization and hydration of TC are reduced, enhancing adsorption probably through hydrogen bonding between the imide groups of the polymer and functional groups on the TC molecules, as well as π–π stacking interactions between the phenyl rings of both host and guest molecules.[50] At higher pH, the adsorption capacity decreases considerably due to the formation of TC^{-} species, which introduces electrostatic repulsion with the electron-rich, negatively charged framework of both polymers.[50]

3.3.2. Impact of dose. Since the highest adsorption capacity was observed at neutral pH, PBS was selected as the medium for subsequent adsorption studies. Fig. 5B illustrates the effect of varying the adsorbent dose on the removal efficiency of each POP at a fixed TC concentration (50 mg L^{-1}). A clear increasing trend was observed, with initial removal efficiencies of 14% and 6% using 0.5 mg of PI-POP and NI-POP, respectively. However, as the adsorbent dose increased, the removal efficiency significantly improved, reaching approximately 85% with 10 mg of PI-POP, with no further significant increase at higher doses (up to ~90% with 15 mg). In contrast, NI-POP showed a more gradual improvement in removal efficiency without reaching a plateau. Since NI-POP did not reach saturation, increasing its dosage further may enhance TC removal beyond the levels observed at 15 mg. A dose of 5 mg of PI-POP achieved approximately 65% TC removal, whereas 15 mg of NI-POP was required to reach a similar removal efficiency. This disparity underscores the superior porosity and larger pore volume of PI-POP, which provide more room for TC capture. Overall, this trend aligns with the principle that increasing the adsorbent dose enhances the collision probability of the polymer particles with TC molecules, therefore improving its TC adsorption efficiency in aqueous solution.[21] When compared to the work published by Zhu *et al.*,[50] under identical conditions—using the same TC concentration and a similar adsorbent-to-TC weight ratio (15 mg of the adsorbent to 0.5 mg of TC)—NI-POP demonstrated a removal efficiency comparable to that of their graphene oxide/calcium alginate composite. However, PI-POP outperformed it by approximately 28%. Similarly, relative to another study conducted by Matias *et al.*,[53] who

employed the same solid-to-liquid ratio (R_{S-L} = 1.5, with 15 mg of the adsorbent in 10 mL of a 50 mg L^{-1} TC solution), both of our polymers exhibited higher adsorption capacities.

Specifically, NI-POP exceeded the performance of the reported triazine-based porous organic polymer by approximately 20%, while PI-POP surpassed it by nearly 65%. These findings underscore the strong potential of both PI-POP and NI-POP as efficient adsorbents for the removal of tetracycline from wastewater.

3.3.3. Impact of contact time. The effect of contact time on adsorption was evaluated by monitoring the changes in the UV-Vis absorbance of the mixture at various time intervals. As shown in Fig. 5C, both polymers exhibited rapid adsorption within the first 6 hours, capturing nearly 80% of their total adsorption capacity. After this initial phase, the adsorption rate gradually declined until equilibrium was reached. Under identical conditions, PI-POP adsorbed a higher amount of TC (~64 mg g^{-1}) over 28 hours compared to NI-POP (~38 mg g^{-1}), aligning with their respective surface area measurements. Despite PI-POP having a ~1.9× higher surface area and double the pore volume, its adsorption capacity is only ~1.7× greater than that of NI-POP. As described in Section 3.2, photoluminescence analysis demonstrated that PI-POP follows the Lehrer model, suggesting that a portion of PI-POP's pores may be inaccessible to TC molecules, possibly due to steric hindrance or structural constraints. This highlights the crucial role of surface area and pore volume in influencing the adsorption performance of these POPs.

Generally, the adsorption kinetics in a solid–liquid system are expected to follow sequential steps: (1) the adsorbate moves from the bulk solution to the adsorbent surface, (2) diffuses through a boundary layer to reach the adsorbent surface, (3) binds to the active adsorption sites on the surface, and (4) undergoes intraparticle diffusion into the internal pores of the adsorbent.[54] To better understand the kinetics, the adsorption behavior of TC onto the polymers was further analyzed using the pseudo-first-order (PFO), pseudo-second-order (PSO), and Elovich models (see Table S1, ESI,† for nonlinear and linear equations).

The pseudo-first-order model did not provide a satisfactory correlation for either polymer, exhibiting the lowest correlation coefficient (R^2) (Fig. S4A and C, ESI†). In contrast, the linear fits (Fig. 6C and Fig. S4B for PI-POP and Fig. 6D and Fig. S4D for NI-POP, ESI†) demonstrated that both Elovich and PSO models

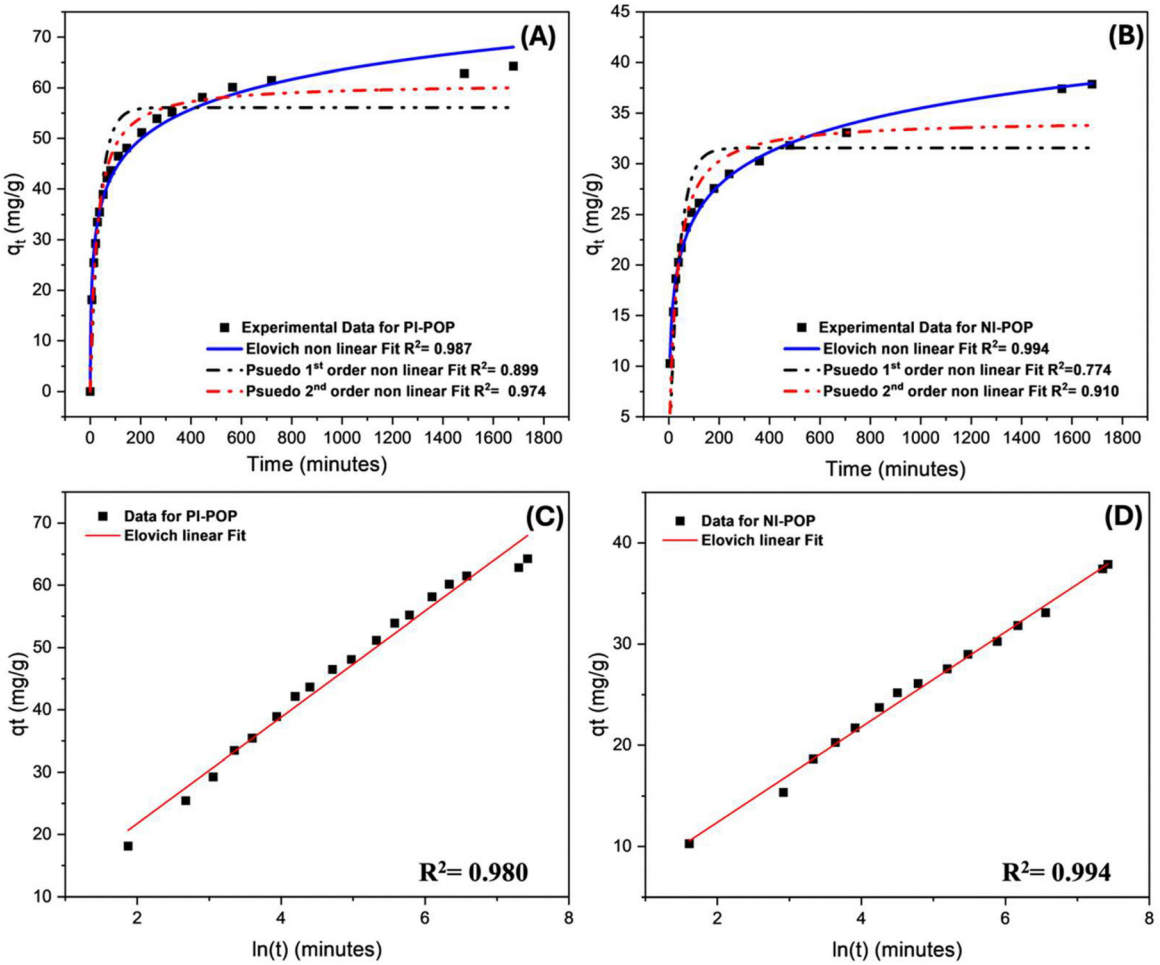

Fig. 6 Plots of adsorption kinetics showing the non-linear fit of the models applied (A) and (B) and the linear fit of the Elovich model, as the best-fitting model among the three employed, for PI-POP (C) and NI-POP (D).

effectively describe the adsorption kinetics, with the PSO model yielding a higher R^2 value for both polymers. However, non-linear fitting is generally preferred over linear fitting, as it avoids distortions and inaccuracies introduced by linearization.[55] Therefore, in this study, non-linear fitting was adopted for more accurate kinetic modeling. The non-linear fit (Fig. 6A and B) exhibited a stronger correlation with the Elovich model (higher R^2 and lower chi-square (χ^2) values; Table S3, ESI†), reinforcing its suitability for describing the adsorption mechanism.

The Elovich model suggests that adsorption occurs on a heterogeneous adsorbent surface, where the adsorption decreases exponentially as the coverage increases.[56] This aligns well with expectations, as both polymers exhibit surface heterogeneity due to the presence of various functional groups, such as triazine rings, imide linkages, and phenyl units. The porous framework further contributes multiple adsorption sites with varying binding affinities for TC molecules.

PI-POP exhibited a higher initial adsorption rate (α = 14.4 mg g^{-1} min^{-1}) compared to NI-POP (α = 8.43 mg g^{-1} min^{-1}), indicating a more rapid occupation of active sites at the early stages of adsorption (Table S3, ESI†). This can be attributed to the higher surface area and more accessible functional groups of PI-POP, which facilitate faster interaction with TC. Furthermore, the lower desorption constant (β = 0.117 g mg^{-1}) observed for PI-POP compared to NI-POP (β = 0.211 g mg^{-1}) implies a higher energy barrier for desorption, reflecting higher affinity and more stable interactions between TC and the polymer surface.

3.3.4. Impact of the initial concentration of TC. The adsorption isotherms were measured by adding 10 mg of the polymer to 20 mL of TC solutions with varying initial concentrations, ranging from 5 to 100 mg L^{-1} for PI-POP and from 5 to 75 mg L^{-1} for NI-POP, given its lower adsorption capacity. For PI-POP, the adsorption capacity steadily increased across the entire concentration range, reaching a q_e of approximately 106 mg g^{-1}, with no indication of saturation (Fig. 5D). This suggests that the adsorption sites were not fully occupied even at an initial concentration (C_0) of 100 mg L^{-1}. In contrast, NI-POP exhibited an adsorption capacity that increased to approximately 45 mg g^{-1} at a C_0 of 50 mg L^{-1} but showed minimal change when C_0 was increased to 75 mg L^{-1}. This plateau indicates the saturation of active sites on NI-POP.[53]

The experimental data were analyzed using three common models in both linear and non-linear forms. Based on the R^2

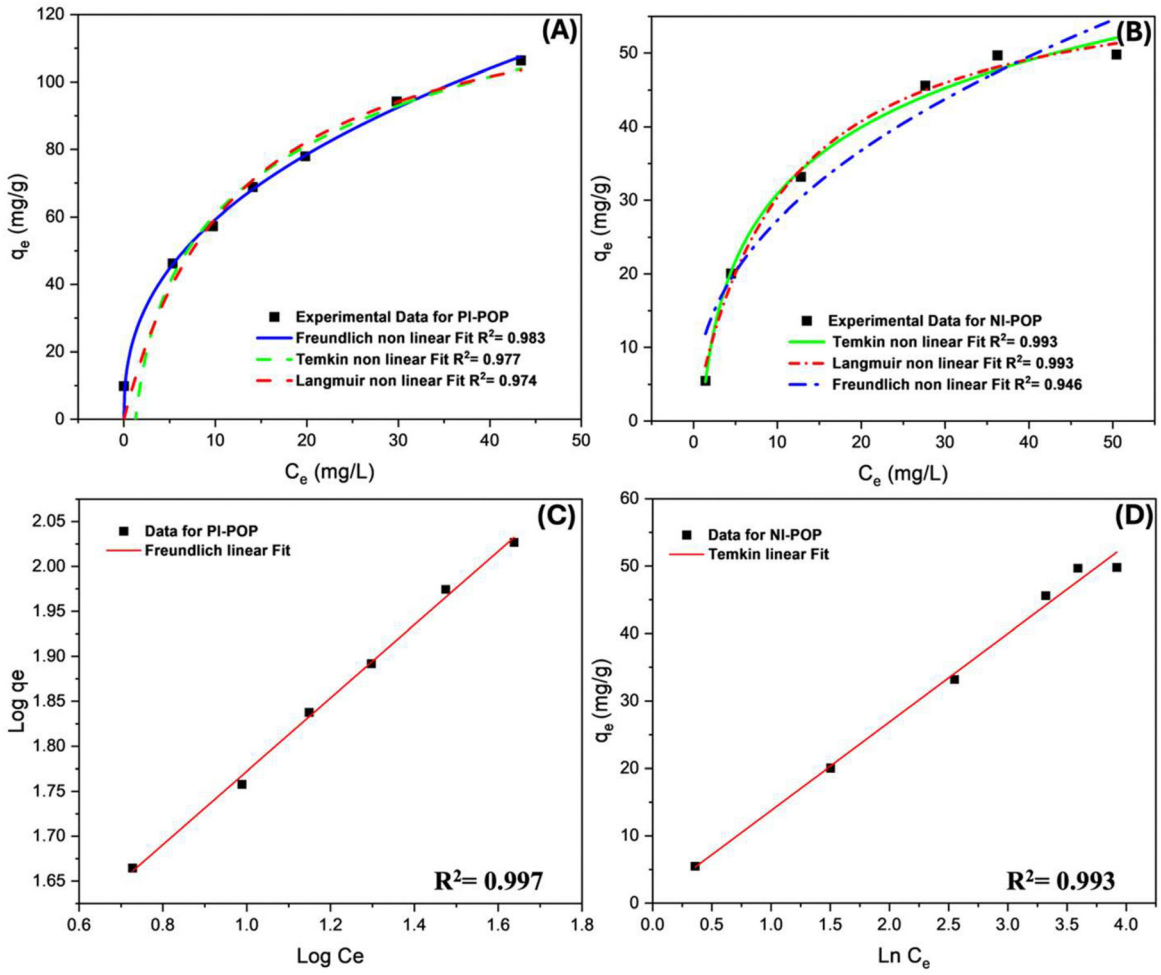

Fig. 7 Adsorption isotherms showing the non-linear fit of the models applied (A) and (B) and the best linear fitting model among the three employed for PI-POP (C) and for NI-POP (D).

and chi-square values (Table S4, ESI†), the Freundlich model provided the best fit for PI-POP across the investigated concentration range in both non-linear and linear forms (Fig. 7A and C), while the Langmuir and Temkin models did not adequately describe the adsorption mechanism of PI-POP (Fig. S5A and B, ESI†). The Freundlich model supports the heterogeneous nature of the adsorbent's surface with varying surface energy,[57] as also suggested earlier by the Elovich model for the kinetic data. Additionally, the Freundlich model assumes multilayer coverage with an infinite adsorption capacity, which could explain the absence of a saturation plateau. The value of n, calculated from the non-linear fit using Origin software (Table S4, ESI†), is greater than 1, indicating favorable adsorption of TC from the aqueous medium.[58] In contrast, NI-POP followed a different adsorption mechanism. When comparing R^2 values, the Freundlich model provided the least accurate fit (Fig. S5C, ESI†), whereas the Langmuir and Temkin non-linear fits (Fig. 7B) were comparable, the R^2 values of both exceeding 0.99 with the Temkin model showing a slightly lower χ^2 value.

However, linear fitting aligned better with the Temkin model (Fig. 7D and Fig. S5D, ESI†), which assumes interactions between the adsorbent and adsorbate on a heterogeneous surface, where active adsorption sites play a significant role.[59,60] Considering the complex nature of the polymers, it is less likely that the adsorption mechanism of NI-POP strictly follows the Langmuir model, which assumes a uniform surface. Instead, the Temkin model appears to be the most plausible for describing the behavior of NI-POP. The Temkin constant, b, related to the heat of adsorption, was determined from the non-linear fit to be 189 J mol^{-1}. This value indicates that the adsorption process is predominantly governed by physisorption, involving diverse electrostatic and van der Waals interactions between the guest and host molecules.[39]

3.4. Applicability in tap water and recyclability

To evaluate the real-world applicability of the synthesized POPs, adsorption experiments were extended to tap water, a more complex matrix compared to buffered systems. A tetracycline solution with an initial concentration of 50 mg L^{-1} was used to assess the performance of polymers under non-ideal conditions. Remarkably, both PI-POP and NI-POP maintained removal efficiencies comparable to those observed in PBS (Table 2). This performance contrasts with the findings of Han *et al.*,[61] where the adsorption capacity of biochar decreased by approximately 20% in tap water. However, it aligns with the observations of Yaqubi *et al.*,[62] who reported enhanced adsorption capability in tap water compared to deionized water.

Table 2 Comparison of the removal percentage of TC (50 mg L^{-1}) from PBS and tap water by both polymers

	Removal%	
Medium	PI-POP	NI-POP
PBS	57.54 ± 2.93	47.86 ± 1.19
Tap water	60.54 ± 1.73	52.02 ± 1.52

The tap water used in this study had a pH of 8.2. Based on the pH study (Fig. 5A), adsorption is typically less favorable under alkaline conditions. Interestingly, the adsorption capacity in tap water did not decline despite the basic pH. Although TC predominantly exists in its anionic form at this pH (>7.7), which could result in electrostatic repulsion from the electron-dense polymer framework, the presence of diverse cationic components (*i.e.* Ca^{2+} and Mg^{2+}) in tap water likely caused surface-bridging between TC ions and the polymer.[63] These cations are presumed to interact with charged sites on the polymer, reducing electrostatic repulsion and facilitating alternative binding mechanisms at neutral sites.[62,63] Consequently, the presence of competing ions and/or natural impurities usually found in tap water did not impair the adsorption performance. This result highlights the robustness and reliability of the materials, reinforcing their potential for practical environmental applications beyond controlled laboratory settings.

For practical applications, an adsorbent should maintain its performance over multiple cycles and be easily regenerated. In this study, each loaded polymer was soaked in ethanol and shaken vigorously at 37 °C for 2 hours. The adsorbent was then filtered, washed excessively with fresh ethanol, and dried for use in another loading cycle. The adsorption/desorption process was conducted over three consecutive cycles, and as shown in Fig. S6 (ESI†), no significant decrease in removal efficiency was observed for either POP over the cycles. These results confirm that both polymers can be effectively regenerated without any noticeable impact on their performance.

3.5. Temperature-dependent release of TC and post-release antibacterial activity

To complete the envisioned cycle of detection, capture, and reuse of TC, the final part of this study focused on evaluating whether the adsorbed tetracycline could be effectively released while retaining its antibacterial activity. Two complementary tests were conducted: (i) a comparative release study at room temperature and physiological temperature (37 °C) to assess temperature-dependent release behavior and (ii) a diffusion test to assess whether the released TC remained structurally intact and biologically active.

The cumulative release profiles of tetracycline from both PI-POP and NI-POP clearly demonstrate a temperature-dependent trend (Fig. 8A and B). It is worth noting that no significant burst release was observed in any case. At 37 °C, both polymers exhibited accelerated release rates compared to RT, indicating the thermally responsive nature of the polymer–drug interactions. The elevated temperatures enhance the molecular mobility, thus allowing leakage of trapped molecules.[64] Relative to NI-POP, the difference between the two conditions for PI-POP was more pronounced, with a markedly higher release at 37 °C, suggesting stronger host–guest interactions that require elevated temperatures to be overcome.

Conversely, NI-POP showed a more gradual release under both conditions, yet achieved a higher overall release percentage, implying a weaker binding affinity with TC, resulting in easier diffusion of TC molecules through the polymer pores. To

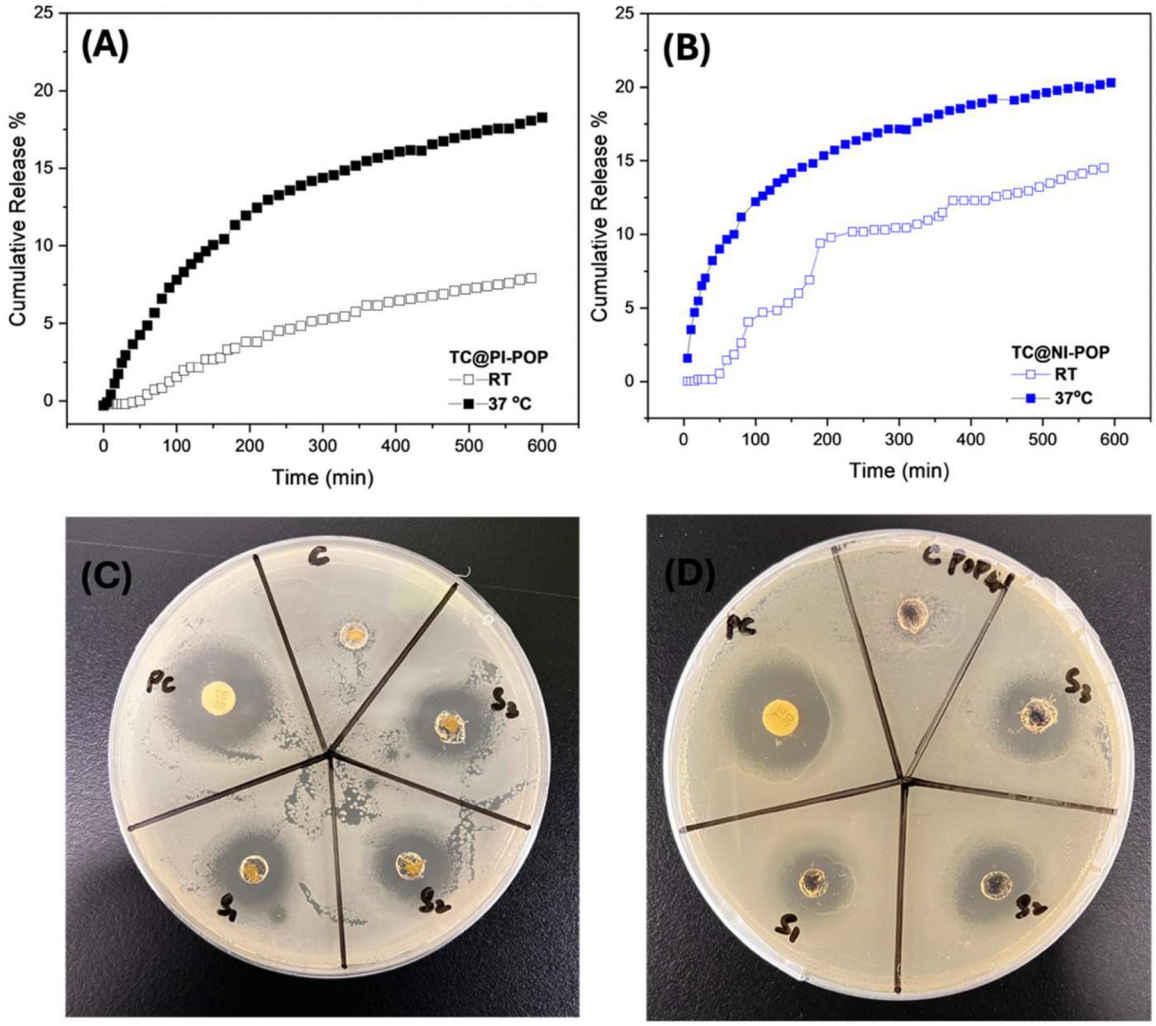

Fig. 8 Temperature-dependent release of TC from PI-POP (A) and NI-POP (B), and diffusion test for TC@PI-POP (C) and TC@NI-POP (D) against EC.

elucidate the mechanism of drug release from the polymer matrices, the experimental release profiles were fitted to widely used kinetic models for polymer-based delivery systems.[65] For PI-POP, the Higuchi model showed the best fit (highest R^2 = 0.98), suggesting that TC release is primarily governed by Fickian diffusion through the porous network without polymer swelling. The release mechanism involves fluid penetration into the matrix, dissolution of the entrapped drug, and its subsequent diffusion into the surrounding medium.[66] In contrast, the release from NI-POP followed the Korsmeyer–Peppas model, with a diffusion exponent (n) value of 0.31. This value (<0.45) indicates a hindered Fickian diffusion regime, where release is still diffusion-driven but occurs through a partially swollen matrix. The diffusion process is likely influenced by internal structural rearrangements within the polymer.[67] Equations and plots for each kinetic model are provided in Table S5 and Fig. S7, S8 (ESI†).

To confirm the structural integrity of the released TC, the UV-Vis absorption spectra were recorded and compared to those of pristine TC in PBS at 37 °C (Fig. S9, ESI†). The spectra showed nearly identical absorption profiles, with only a slight broadening in the first peak in the case of NI-POP, attributed to the relatively lower concentration of released TC. This spectral overlap confirms that the released TC remained chemically intact after polymer interaction.

Furthermore, to investigate the antibacterial activity of the released TC, their ability to inhibit EC (Fig. 8C and D) and SE bacteria (Fig. S10A and B, ESI†) was tested using the agar diffusion method. In each case, 1 mg of the TC-loaded polymer was placed on a seeded Petri dish and incubated for 24 h. The resulting inhibition zones were measured and compared to two controls: (i) a 30 μg TC disc (positive control) and (ii) 1 mg of the unloaded polymer (negative control). Both PI-POP and NI-POP produced clear zones of inhibition against EC and SE, while the unloaded polymers showed no antibacterial effect. The slightly smaller inhibition diameters compared to the TC disc (Table 3) are consistent with the sustained release behavior observed in the temperature-dependent release studies, where a maximum of ~20% of the loaded drug (in the case of NI-POP) was released within 10 hours.

Interestingly, despite PI-POP having demonstrated superior adsorption performance in earlier experiments (Section 3.3),

Table 3 Diameter of bacterial growth inhibition on a Petri dish by the TC-loaded polymers

	Average diameter of bacterial growth inhibition (cm)	
Name of the sample	EC	SE
PI-POP	1.27 ± 0.047	1.57 ± 0.047
NI-POP	1.40 ± 0.14	1.50 ± 0.082
Positive control (TC disc)	1.95	2.10
Negative control (POP)	0	0

the release from NI-POP led to larger inhibition zones in EC and comparable ones in SE. This can be attributed to the weaker interaction strength between TC and NI-POP—as suggested by both the sensing response (Section 3.2) and the release profiles—which facilitated more efficient TC diffusion even at room temperature. These observations highlight the influence of the polymer structure on drug retention and release kinetics.

Conclusion

In this study, two polyimide-based porous organic polymers, PI-POP and NI-POP, were synthesized and evaluated as multifunctional materials for the detection, capture, and controlled release of tetracycline. Both polymers possess π-rich frameworks, abundant functional groups, and hybrid micro-mesoporous structures with moderate surface areas, enabling their application in diverse functions. Fluorescence quenching experiments revealed that both PI-POP and NI-POP are capable of detecting TC at low concentrations, with PI-POP showing a more pronounced response—indicating stronger polymer–analyte interactions. Following detection, the adsorption performance of the polymers was systematically studied. Optimal removal was achieved under neutral pH conditions and increasing the polymer dosage significantly enhanced the adsorption efficiency. PI-POP achieved ∼90% removal at a solid–liquid ratio of 1.5, outperforming NI-POP, largely due to its higher surface area and pore volume.

The practical applicability of both polymers was confirmed in tap water, where removal efficiencies remained comparable to those in buffered systems. Finally, the release behavior of TC from the loaded polymers was investigated at room and physiological temperatures. Both polymers exhibited sustained release of TC over time with NI-POP showing a higher cumulative release, attributed to weaker drug–polymer interactions. Importantly, the released TC retained its antibacterial efficacy as demonstrated by clear zones of inhibition in agar diffusion assays. These results highlight the multifunctional capability of PI-POP and NI-POP, offering an integrated platform for antibiotic detection, environmental remediation, and therapeutic reuse.

Author contributions

Rasha Diab: conceptualization, methodology, visualization, investigation, writing – original draft; Fatima Mahroos: methodology, investigation; Sreeshna Ravindran: methodology, investigation; Oussama M. El-Kadri: conceptualization, supervision, writing – review & editing, funding acquisition; Mohammad H. Al-Sayah: conceptualization, supervision, writing – review & editing, funding acquisition.

Conflicts of interest

The authors declare no competing interests.

Data availability

All data supporting this research are included in the manuscript and the ESI.†

Acknowledgements

This research was supported by the American University of Sharjah (FRG23-C-S64 and FRG23-E-S76). The work presented in this paper was supported, in part, by the Open Access Program from the American University of Sharjah (OPFY25-3152-OC2529). This paper represents the opinions of the authors and does not mean to represent the position or opinions of the American University of Sharjah.

References

1 D. G. J. Larsson and C. F. Flach, Antibiotic Resistance in the Environment, *Nat. Rev. Microbiol.*, 2021, **20**(5), 257, DOI: 10.1038/S41579-021-00649-X.
2 Z. A. Mumtaj, A. R. Khan, J. A. Ansari, A. Asiri and S. Khan, A Brief Overview of Antibiotic Contamination Sources in Wastewater and Elimination Approaches, *Rocz. Ochr. Sr*, 2024, **26**, 201–216, DOI: 10.54740/ros.2024.021.
3 E. S. Okeke, K. I. Chukwudozie, R. Nyaruaba, R. E. Ita, A. Oladipo, O. Ejeromedoghene, E. O. Atakpa, C. V. Agu and C. O. Okoye, Antibiotic Resistance in Aquaculture and Aquatic Organisms: A Review of Current Nanotechnology Applications for Sustainable Management, *Environ. Sci. Pollut. Res.*, 2022, **29**(46), 69241–69274, DOI: 10.1007/S11356-022-22319-Y.
4 L. O. Omuferen, B. Maseko and J. O. Olowoyo, Occurrence of Antibiotics in Wastewater from Hospital and Convectional Wastewater Treatment Plants and Their Impact on the Effluent Receiving Rivers: Current Knowledge between 2010 and 2019, *Environ. Monit. Assess.*, 2022, **194**(4), 1–25, DOI: 10.1007/S10661-022-09846-4/TABLES/3.
5 V. Sonkar, V. Venu, B. Nishil and S. Thatikonda, Review on Antibiotic Pollution Dynamics: Insights to Occurrence, Environmental Behaviour, Ecotoxicity, and Management Strategies, *Environ. Sci. Pollut. Res.*, 2024, **31**(39), 51164–51196, DOI: 10.1007/S11356-024-34567-1.
6 V. Lopez-Chavarrias, M. Ugarte-Ruiz, C. Barcena, A. Olarra, M. Garcia, J. L. Saez, C. de Frutos, T. Serrano, I. Perez, M. A. Moreno, L. Dominguez and J. Alvarez, Monitoring of Antimicrobial Resistance to Aminoglycosides and Macrolides in Campylobacter Coli and Campylobacter Jejuni From

Healthy Livestock in Spain (2002–2018, *Front. Microbiol.*, 2021, 12, DOI: 10.3389/fmicb.2021.689262.
7 D. Chinemerem Nwobodo, M. C. Ugwu, C. Oliseloke Anie, M. T. S. Al-Ouqaili, J. Chinedu Ikem, U. Victor Chigozie and M. Saki, Antibiotic Resistance: The Challenges and Some Emerging Strategies for Tackling a Global Menace, *J. Clin. Lab. Anal.*, 2022, **36**(9), e24655, DOI: 10.1002/JCLA.24655.
8 A. Thakali and J. D. MacRae, A Review of Chemical and Microbial Contamination in Food: What Are the Threats to a Circular Food System?, *Environ. Res.*, 2021, **194**, 110635, DOI: 10.1016/J.ENVRES.2020.110635.
9 F. Liu, Y. Ge, Y. Wei, D. Xing, N. Ren and S. H. Ho, Multicolor Fluorescence Strategy for Rapid and Simultaneous Detection of Antibiotics in Wastewaters and the Entire Process Detection Mechanisms, *Sens. Actuators, B*, 2025, **423**, 136726, DOI: 10.1016/J.SNB.2024.136726.
10 M. Getahun, R. B. Abebe, A. K. Sendekie, A. E. Woldeyohanis and A. E. Kasahun, Evaluation of Antibiotics Residues in Milk and Meat Using Different Analytical Methods, *Int. J. Anal. Chem.*, 2023, **2023**(1), 4380261, DOI: 10.1155/2023/4380261.
11 Z. Zhang, H. Zhang, D. Tian, A. Phan, M. Seididamyeh, M. Alanazi, Z. Ping Xu, Y. Sultanbawa and R. Zhang, Luminescent Sensors for Residual Antibiotics Detection in Food: Recent Advances and Perspectives, *Coord. Chem. Rev.*, 2024, **498**, 215455, DOI: 10.1016/J.CCR.2023.215455.
12 Q. Chen, M. Gao, M. Yu, T. Zhang, J. Wang, J. Bi and F. Dong, Efficient Photo-Degradation of Antibiotics by Waste Eggshells Derived AgBr-CaCO3 Heterostructure under Visible Light, *Sep. Purif. Technol.*, 2023, **314**, 123573, DOI: 10.1016/J.SEPPUR.2023.123573.
13 S. Shao, Y. Hu, J. Cheng and Y. Chen, Degradation of Oxytetracycline (OTC) and Nitrogen Conversion Characteristics Using a Novel Strain, *Chem. Eng. J.*, 2018, **354**, 758–766, DOI: 10.1016/j.cej.2018.08.032.
14 A. D. Khatibi, A. H. Mahvi, N. Mengelizadeh and D. Balarak, Adsorption-Desorption of Tetracycline onto Molecularly Imprinted Polymer: Isotherm, Kinetics and Thermodynamics Studies, *Desalin. Water Treat.*, 2021, **230**, 240–251, DOI: 10.5004/dwt.2021.27396.
15 A. Shahbazi, A. H. Hamidian, Y. Zhang and M. Yang, Adsorption of Fluoroquinolone Antibiotics in Aqueous Solutions Using Nanomaterials: Mechanisms, Challenges, and Future Perspectives, *Nanotechnol. Environ. Eng.*, 2025, **10**, 25, DOI: 10.1007/S41204-025-00417-9.
16 N. Mamidi, R. M. V. Delgadillo, A. O. Sustaita, K. Lozano and M. M. Yallapu, Current Nanocomposite Advances for Biomedical and Environmental Application Diversity, *Med. Res. Rev.*, 2025, **45**(2), 576–628, DOI: 10.1002/MED.22082.
17 N. Mamidi, R. G. García, J. D. H. Martínez, C. M. Briones, A. M. Martínez Ramos, M. F. L. Tamez, B. G. Del Valle and F. J. M. Segura, Recent Advances in Designing Fibrous Biomaterials for the Domain of Biomedical, Clinical, and Environmental Applications, *ACS Biomater. Sci. Eng.*, 2022, **8**(9), 3690–3716, DOI: 10.1021/ACSBIOMATERIALS.2C00786/ASSET/IMAGES/MEDIUM/AB2C00786_0014.GIF.
18 N. Mamidi and R. M. Delgadillo, New Zein Protein Composites with High Performance in Phosphate Removal, Intrinsic Antibacterial, and Drug Delivery Capabilities, *ACS Appl. Mater. Interfaces*, 2024, **16**(29), 37468–37485, DOI: 10.1021/ACSAMI.4C04718/ASSET/IMAGES/LARGE/AM4C04718_0010.JPEG.
19 Y. Zhu, P. Xu, X. Zhang and D. Wu, Emerging Porous Organic Polymers for Biomedical Applications, *Chem. Soc. Rev.*, 2022, **51**(4), 1377–1414, DOI: 10.1039/D1CS00871D.
20 N. Naz, M. H. Manzoor, S. M. G. Naqvi, U. Ehsan, M. Aslam and F. Verpoort, Porous Organic Polymers; an Emerging Material Applied in Energy, Environmental and Biomedical Applications, *Appl. Mater. Today*, 2024, **38**, 102198, DOI: 10.1016/J.APMT.2024.102198.
21 W. Nie, J. Liu, X. Bai, Z. Xing and Y. Gao, Designing Phenyl Porous Organic Polymers with High-Efficiency Tetracycline Adsorption Capacity and Wide PH Adaptability, *Polymers*, 2022, **14**(1), 203, DOI: 10.3390/polym14010203.
22 B. Mohan, A. Shanmughan, A. V. Krishna, M. K. Noushija, D. Umadevi and S. Shanmugaraju, Porous Organic Polymers-Based Fluorescent Chemosensors for Fe(III) Ions-a Functional Mimic of Siderophores, *Front. Chem.*, 2024, **12**, 1361796, DOI: 10.3389/FCHEM.2024.1361796/BIBTEX.
23 Y. Liu, H. Zhou, X. Zhou, C. Jin, G. Liu, S. Huo, F. Chu and Z. Kong, Natural Phenol-Inspired Porous Polymers for Efficient Removal of Tetracycline: Experimental and Engineering Analysis, *Chemosphere*, 2023, **316**, 137798, DOI: 10.1016/J.CHEMOSPHERE.2023.137798.
24 Z. Xu, L. Hu, J. Ming, X. Cui, M. Zhang, J. Dou, W. Zhang and B. Zhou, Self-Gated Porous Organic Polymer as Drug Delivery System for PH Stimuli-Responsive Controlled Quercetin Release, *Microporous Mesoporous Mater.*, 2020, **303**, 110259, DOI: 10.1016/J.MICROMESO.2020.110259.
25 R. Daghrir and P. Drogui, Tetracycline Antibiotics in the Environment: A Review, *Environ. Chem. Lett.*, 2013, **11**(3), 209–227, DOI: 10.1007/s10311-013-0404-8.
26 M. E. Cañas-Ventura, W. Xiao, D. Wasserfallen, K. Müllen, H. Brune, J. V. Barth and R. Fasel, Self-Assembly of Periodic Bicomponent Wires and Ribbons, *Angew. Chem., Int. Ed.*, 2007, **46**(11), 1814–1818, DOI: 10.1002/ANIE.200604083.
27 R. Diab, G. Boltaev, M. M. Kaid, A. Fawad, H. M. El-Kaderi, M. H. Al-Sayah, A. S. Alnaser and O. M. El-Kadri, Fabrication of Heteroatom-Doped Graphene-Porous Organic Polymer Hybrid Materials via Femtosecond Laser Writing and Their Application in VOCs Sensing, *Sci. Rep.*, 2025, **15**(1), 1–14, DOI: 10.1038/s41598-025-87681-6.
28 Z. Wang, B. Zhang, H. Yu, L. Sun, C. Jiao and W. Liu, Microporous Polyimide Networks with Large Surface Areas and Their Hydrogen Storage Properties, *Chem. Commun.*, 2010, **46**(41), 7730–7732, DOI: 10.1039/C0CC02489A.
29 J. X. Jiang, F. Su, A. Trewin, C. D. Wood, H. Niu, J. T. A. Jones, Y. Z. Khimyak and A. I. Cooper, Synthetic Control of the Pore Dimension and Surface Area in Conjugated Microporous Polymer and Copolymer Networks, *J. Am. Chem. Soc.*, 2008, **130**(24), 7710–7720, DOI: 10.1021/JA8010176/SUPPL_FILE/JA8010176-FILE002.PDF.

30 D. Wang; W. Yang; S. Feng and H. Liu Hybrid Porous Polymers Derived from Cubic Octavinylsilsequioxane and Planar Halogenated Benzene Monomers Exhibit High Thermal Stability, Tunable Porosities and Potential Applications in Carbon Dioxide Storage. ARTICLE TYPE Constructing Hybrid Porous Polymers from Cubic Octavinylsilsequioxane and Planar Halogenated Benzene † Received (in XXX, XXX) Xth XXXXXXXXX 20XX, Accepted Xth XXXXXXXXX 20XX, DOI: 10.1039/c0xx00000x.

31 Y. Luo, B. Li, L. Liang and B. Tan, Synthesis of Cost-Effective Porous Polyimides and Their Gas Storage Properties, *Chem. Commun.*, 2011, **47**(27), 7704–7706, DOI: 10.1039/C1CC11466B.

32 S. H. Hsiao, W. Guo, Y. C. Kung and Y. J. Lee, Redox-Active and Electrochromic Aromatic Poly(Amide-Imide)s with 2,4-Dimethoxytriphenylamine Chromophores, *J. Polym. Res.*, 2011, **18**(6), 1353–1364, DOI: 10.1007/S10965-010-9538-6/FIGURES/10.

33 IR Spectroscopy of Hydrocarbons Hydrocarbons Contain Only Carbon–Carbon Bonds and Carbon-Hydrogen Bonds.

34 K. M. Jeong, Y. Li, D. G. Yoo, N. K. Lee, H. G. Lee, S. Ando and C. S. Ha, Effects of Crosslinking Agents on the Physical Properties of Polyimide/Amino-Functionalized Graphene Oxide Hybrid Films, *Polym. Int.*, 2018, **67**(5), 588–597, DOI: 10.1002/PI.5555.

35 B. L. Frey and R. M. Corn, Covalent Attachment and Derivatization of Poly(l-Lysine) Monolayers on Gold Surfaces As Characterized by Polarization−Modulation FT-IR Spectroscopy, *Anal. Chem.*, 1996, **68**(18), 3187–3193, DOI: 10.1021/AC9605861.

36 S. Das, P. Heasman, T. Ben and S. Qiu, Porous Organic Materials: Strategic Design and Structure-Function Correlation, *Chem. Rev.*, 2017, **117**(3), 1515–1563, DOI: 10.1021/ACS.CHEMREV.6B00439/ASSET/IMAGES/MEDIUM/CR-2016-004399_0056.GIF.

37 K. Sing, The Use of Nitrogen Adsorption for the Characterisation of Porous Materials, *Colloids Surf., A*, 2001, **187–188**, 3–9, DOI: 10.1016/S0927-7757(01)00612-4.

38 S. Chakraborty, Y. J. Colón, R. Q. Snurr and S. T. Nguyen, Hierarchically Porous Organic Polymers: Highly Enhanced Gas Uptake and Transport through Templated Synthesis, *Chem. Sci.*, 2014, **6**(1), 384–389, DOI: 10.1039/C4SC02502D.

39 S. Wang, Q. Hu, Y. Liu, X. Meng, Y. Ye, X. Liu, X. Song and Z. Liang, Multifunctional Conjugated Microporous Polymers with Pyridine Unit for Efficient Iodine Sequestration, Exceptional Tetracycline Sensing and Removal, *J. Hazard. Mater.*, 2020, **387**, 121949, DOI: 10.1016/J.JHAZMAT.2019.121949.

40 H. S. Geethanjali, D. Nagaraja, R. M. Melavanki and R. A. Kusanur, Fluorescence Quenching of Boronic Acid Derivatives by Aniline in Alcohols – A Negative Deviation from Stern–Volmer Equation, *J. Lumin.*, 2015, **167**, 216–221, DOI: 10.1016/J.JLUMIN.2015.06.040.

41 S. M. Saleh, R. Ali and O. S. Wolfbeis, Quenching of the Luminescence of Upconverting Luminescent Nanoparticles by Heavy Metal Ions, *Chemistry*, 2011, **17**(51), 14611–14617, DOI: 10.1002/CHEM.201101860.

42 Y. Ma, Y. Cen, M. Sohail, G. Xu, F. Wei, M. Shi, X. Xu, Y. Song, Y. Ma and Q. Hu, A Ratiometric Fluorescence Universal Platform Based on N, Cu Codoped Carbon Dots to Detect Metabolites Participating in H2O2-Generation Reactions, *ACS Appl. Mater. Interfaces*, 2017, **9**(38), 33011–33019, DOI: 10.1021/ACSAMI.7B10548/ASSET/IMAGES/LARGE/AM-2017-10548G_0006.JPEG.

43 J. Wang, Y. Qin, Y. Ma, M. Meng and Y. Xu, Low-Toxicity and High-Stability Fluorescence Sensor for the Selective, Rapid, and Visual Detection Tetracycline in Food Samples, *Molecules*, 2024, **29**(24), 5888, DOI: 10.3390/MOLECULES29245888.

44 M. Nagy, D. Rácz, L. Lázár, M. Purgel, T. Ditrói, M. Zsuga and S. Kéki, Solvatochromic Study of Highly Fluorescent Alkylated Isocyanonaphthalenes, Their π-Stacking, Hydrogen-Bonding Complexation, and Quenching with Pyridine, *ChemPhysChem*, 2014, **15**(16), 3614–3625, DOI: 10.1002/CPHC.201402310.

45 Y. Gao, Y. Li, L. Zhang, H. Huang, J. Hu, S. M. Shah and X. Su, Adsorption and Removal of Tetracycline Antibiotics from Aqueous Solution by Graphene Oxide, *J. Colloid Interface Sci.*, 2012, **368**(1), 540–546, DOI: 10.1016/J.JCIS.2011.11.015.

46 A. Sharma, D. Kim, J. H. Park, S. Rakshit, J. Seong, G. H. Jeong, O. H. Kwon and M. S. Lah, Mechanistic Insight into the Sensing of Nitroaromatic Compounds by Metal-Organic Frameworks, *Commun. Chem.*, 2019, **2**(1), 1–8, DOI: 10.1038/s42004-019-0135-2.

47 N. García-Criado, L. Martín-Pozo, J. Martín, J. L. Santos, I. Aparicio and E. Alonso, Efficient Removal of Tetracyclines and Their Metabolites from Wastewater Using Purified Stevensite: Adsorption Capacity, Reusability, and Antibiotic Decontamination, *Antibiotics*, 2025, **14**(4), 395, DOI: 10.3390/ANTIBIOTICS14040395/S1.

48 S. Sağlam, F. N. Türk and H. Arslanoğlu, Tetracycline (TC) Removal from Wastewater with Activated Carbon (AC) Obtained from Waste Grape Marc: Activated Carbon Characterization and Adsorption Mechanism, *Environ. Sci. Pollut. Res.*, 2024, **31**(23), 33904–33923, DOI: 10.1007/S11356-024-33493-6/METRICS.

49 M. Xu, N. Song, D. Qiu, X. Li, Y. Liu, L. Yang, D. Zhang and Z. Zhou, A Porous and Chemical Stable Co(II)-Based Metal-Organic Framework for the Selective Fluorescence Sensing of Fe3+ and Tetracycline, *J. Solid State Chem.*, 2024, **332**, 124562, DOI: 10.1016/J.JSSC.2024.124562.

50 H. Zhu, T. Chen, J. Liu and D. Li, Adsorption of Tetracycline Antibiotics from an Aqueous Solution onto Graphene Oxide/Calcium Alginate Composite Fibers, *RSC Adv.*, 2018, **8**(5), 2616–2621, DOI: 10.1039/C7RA11964J.

51 Z. Li, L. Schulz, C. Ackley and N. Fenske, Adsorption of Tetracycline on Kaolinite with PH-Dependent Surface Charges, *J. Colloid Interface Sci.*, 2010, **351**(1), 254–260, DOI: 10.1016/J.JCIS.2010.07.034.

52 J. Chang, Z. Shen, X. Hu, E. Schulman, C. Cui, Q. Guo and H. Tian, Adsorption of Tetracycline by Shrimp Shell Waste from Aqueous Solutions: Adsorption Isotherm, Kinetics Modeling, and Mechanism, *ACS Omega*, 2020, **5**(7), 3467–3477, DOI: 10.1021/ACSOMEGA.9B03781/ASSET/IMAGES/MEDIUM/AO9B03781_M006.GIF.

53 P. M. C. Matias, S. C. C. Nunes, A. C. B. Rodrigues, M. Ltayef, L. Sellaoui, M. Mbarek, D. Murtinho, A. A. C. Canelas Pais and A. J. M. Valente, Efficient Removal of Sulfonamide and Tetracycline Antibiotics Using Triazine-Based Porous Organic Polymers, *Sep. Purif. Technol.*, 2025, **355**, 129731, DOI: **10.1016/J.SEPPUR.2024.129731**.

54 C. Peiris, S. R. Gunatilake, T. E. Mlsna, D. Mohan and M. Vithanage, Biochar Based Removal of Antibiotic Sulfonamides and Tetracyclines in Aquatic Environments: A Critical Review, *Bioresour. Technol.*, 2017, **246**, 150–159, DOI: **10.1016/J.BIORTECH.2017.07.150**.

55 J. Lin and L. Wang, Comparison between Linear and Non-Linear Forms of Pseudo-First-Order and Pseudo-Second-Order Adsorption Kinetic Models for the Removal of Methylene Blue by Activated Carbon, *Front. Environ. Sci. Eng. China*, 2009, **3**(3), 320–324, DOI: **10.1007/S11783-009-0030-7/METRICS**.

56 G. W. Kajjumba, S. Emik, A. Öngen, H. K. Özcan and S. Aydın, Modelling of Adsorption Kinetic Processes—Errors, Theory and Application. *Advanced Sorption Process Applications*, 2018, DOI: **10.5772/INTECHOPEN.80495**.

57 J. Yang, X. Liu, K. Song, X. Li and D. Wang, Effectively Removing Tetracycline from Water by Nanoarchitectured Carbons Derived from CO2: Structure and Surface Chemistry Influence, *Environ. Res.*, 2021, **195**, 110883, DOI: **10.1016/J.ENVRES.2021.110883**.

58 A. Hu, W. Zhang, Q. You, B. Men, G. Liao and D. Wang, A Green and Low-Cost Strategy to Synthesis of Tunable Pore Sizes Porous Organic Polymers Derived from Waste-Expanded Polystyrene for Highly Efficient Removal of Organic Contaminants, *Chem. Eng. J.*, 2019, **370**, 251–261, DOI: **10.1016/J.CEJ.2019.03.207**.

59 A. Samadi, L. Kong, W. Guo, M. Sillanpää, I. Boztepe, C. Song, Q. Zeng and S. Zhao, Standardized Methodology for Performance Evaluation in Using Polyaniline-Based Adsorbents to Remove Aqueous Contaminants, *J. Environ. Chem. Eng.*, 2024, **12**(3), 112650, DOI: **10.1016/J.JECE.2024.112650**.

60 H. H. Dang, D. T. C. Nguyen, T. T. Nguyen, T. T. T. Nguyen, D. V. N. Vo, T. D. Nguyen, T. Lee and T. V. Tran, Zeolitic-Imidazolate Framework-Derived N-Self-Doped Porous Carbons with Ultrahigh Theoretical Adsorption Capacities for Tetracycline and Ciprofloxacin, *J. Environ. Chem. Eng.*, 2021, **9**(1), 104938, DOI: **10.1016/J.JECE.2020.104938**.

61 R. Han, Y. Song, J. Duan and S. Ai, A Recyclable Biochar with Ultrahigh Absorption Ability for Efficient Removal of Tetracycline Hydrochloride, *Colloids Surf., A*, 2024, **702**, 134974, DOI: **10.1016/J.COLSURFA.2024.134974**.

62 O. Yaqubi, M. H. Tai, D. Mitra, C. Gerente, K. G. Neoh, C. H. Wang and Y. Andres, Adsorptive Removal of Tetracycline and Amoxicillin from Aqueous Solution by Leached Carbon Black Waste and Chitosan-Carbon Composite Beads, *J. Environ. Chem. Eng.*, 2021, **9**(1), 104988, DOI: **10.1016/J.JECE.2020.104988**.

63 M. E. Parolo, M. J. Avena, G. R. Pettinari and M. T. Baschini, Influence of Ca2+ on Tetracycline Adsorption on Montmorillonite, *J. Colloid Interface Sci.*, 2012, **368**(1), 420–426, DOI: **10.1016/J.JCIS.2011.10.079**.

64 Y. Hu, I. Kim, Y.; Jeong, J. pil; Park, S.; Shin, Y.; Ki Hong, M. Sung Kim and S. Jung, Novel Temperature/PH-Responsive Hydrogels Based on Succinoglycan/Poly(N-Isopropylacrylamide) with Improved Mechanical and Swelling Properties, *Eur. Polym. J.*, 2022, **174**, 111308, DOI: **10.1016/J.EURPOLYMJ.2022.111308**.

65 S. Kini, D. Bahadur and D. Panda, Mechanism of Anti-Cancer Activity of Benomyl Loaded Nanoparticles in Multidrug Resistant Cancer Cells, *J. Biomed. Nanotechnol.*, 2015, **11**(5), 877–889, DOI: **10.1166/JBN.2015.1998**.

66 Y. Zhou, J. S. Chu, J. X. Li and X. Y. Wu, Theoretical Analysis of Release Kinetics of Coated Tablets Containing Constant and Non-Constant Drug Reservoirs, *Int. J. Pharm.*, 2010, **385**(1–2), 98–103, DOI: **10.1016/j.ijpharm.2009.10.039**.

67 M. C. Rosu and I. Bratu, Promising Psyllium-Based Composite Containing TiO2 Nanoparticles as Aspirin-Carrier Matrix, *Prog. Nat. Sci.:Mater. Int.*, 2014, **24**(3), 205–209, DOI: **10.1016/J.PNSC.2014.05.007**.